Anal. Chem. **2007,** *79,* 8316−8322

Free-Solution Oligonucleotide Separation in Nanoscale Channels

Sumita Pennathur, Fabio Baldessari, and Juan G. Santiago*

Mechanical Engineering Department, Stanford University, Stanford, California 94305

Michael G. Kattah, Jonathan B. Steinman, and Paul J. Utz

Medicine—Immunology and Rheumatology, Stanford University, Stanford, California 94305

In this paper, we report an experimental study of electrokinetic transport and separation of double-stranded deoxyribonucleic acid (dsDNA) oligonucleotides in custom-fabricated fused-silica nanochannels filled with a gel-free sodium borate aqueous buffer. Mixtures of fluorescently labeled dsDNA molecules in the range of 10−100 base pair (bp), fluorescein, and fluorescein-12-UTP (UTP) were separated in less than 120 s in channels of depth ranging from 40 to 1560 nm. We varied the channel depth and background buffer concentration to achieve a 0.006−0.2 range of Debye length-to-channel-half-depth ratio (λ_D/h), and a 0.004−1.7 range of the ratio of length of dsDNA molecule to channel half-depth (l/h). We find observed oligonucleotide migration times depend on both l/h and λ_D/h. Electrophoretic mobility estimates agree well with published (micrometer-scale channel) values for background electrolyte (BGE) concentrations greater than approximately 10 mM. At BGE concentrations of 1 and 5 mM, mobility estimates in our nanochannels are higher than published values. Of the cases studied, the highest separation sensitivities were achieved in 100 nm channels with 1−10 mM ion density buffers. Potential applications of this technology include rapid small-scale sequencing and other fluorescence-based oligonucleotide separation and detection assays.

Efficient, selective, and fast separation methods are needed to meet the challenges of nucleic acid synthesis, separation, detection, and analysis.[1] Therapeutic applications include antisense oligonucleotide sensing and analysis of small interfering RNA. Molecular biology applications range from single-nucleotide polymorphism assays to micro-RNA studies.[2] Oligonucleotides are routinely used in both clinical and research laboratories as primers for the amplification of DNA by the polymerase chain reaction (PCR). Currently, the two major techniques that are used for the separation of oligonucleotides are electrophoresis (both slab gel and capillary gel models)[3−5] and high-performance liquid chromatography (HPLC).[6−10] Although these methods are adequate for conventional applications, the growing need for reduced reagent consumption, parallel analysis, higher throughput, more sensitive detection, and higher resolution can greatly benefit from novel miniaturized electrophoresis systems.[11−13] These systems have the potential to substantially increase the speed and throughput of automated DNA analysis while reducing the overall cost per assay.[14]

In the past 5 years, there have been numerous reports of microscale DNA separation methods.[1,15−25] The most notable

* To whom correspondence should be addressed. E-mail: juan.santiago@stanford.edu.

(1) Chou, C. F.; Austin, R. H.; Bakajin, O.; Tegenfeldt, J. O.; Castelino, J. A.; Chan, S. S.; Cox, E. C.; Craighead, H.; Darnton, N.; Duke, T.; Han, J. Y.; Turner, S. *Electrophoresis* **2000**, *21*, 81−90.
(2) Zamore, P. D.; Haley, B. *Science* **2005**, *309*, 1519−1524.
(3) Cohen, A. S.; Vilenchik, M.; Dudley, J. L.; Gemborys, M. W.; Bourque, A. J. *J. Chromatogr.* **1993**, *638*, 293−301.
(4) Srivatsa, G. S.; Klopchin, P.; Batt, M.; Feldman, M.; Carlson, R. H.; Cole, D. L. *J. Pharm. Biomed. Anal.* **1997**, *16*, 619−630.
(5) Paulus, A.; Ohms, J. I. *J. Chromatogr.* **1990**, *507*, 113−123.
(6) Agrawal, S.; Tang, J. Y.; Brown, D. M. *J. Chromatogr.* **1990**, *509*, 396−399.
(7) Bergot, B. J.; Egan, W. *J. Chromatogr.* **1992**, *599*, 35−42.
(8) Cohen, A. S.; Najarian, D. R.; Paulus, A.; Guttman, A.; Smith, J. A.; Karger, B. L. *Proc. Natl. Acad. Sci. U.S.A.* **1988**, *85*, 9660−9663.
(9) Heiger, D. N.; Cohen, A. S.; Karger, B. L. *J. Chromatogr.* **1990**, *516*, 33−48.
(10) Metelev, V.; Agrawal, S. *Anal. Biochem.* **1992**, *200*, 342−346.
(11) Collins, F. S.; Green, E. D.; Guttmacher, A. E.; Guyer, M. S. *Nature* **2003**, *422*, 835−847.
(12) Chan, E. Y. *Mutat. Res.* **2005**, *573*, 13−40.
(13) Venter, J. C.; Adams, M. D.; Myers, E. W.; Li, P. W.; Mural, R. J.; Sutton, G. G.; Smith, H. O.; Yandell, M.; Evans, C. A.; Holt, R. A.; Gocayne, J. D.; Amanatides, P.; Ballew, R. M.; Huson, D. H.; Wortman, J. R.; Zhang, Q.; Kodira, C. D.; Zheng, X. Q. H.; Chen, L.; Skupski, M.; Subramanian, G.; Thomas, P. D.; Zhang, J. H.; Miklos, G. L. G.; Nelson, C.; Broder, S.; Clark, A. G.; Nadeau, C.; McKusick, V. A.; Zinder, N.; Levine, A. J.; Roberts, R. J.; Simon, M.; Slayman, C.; Hunkapiller, M.; Bolanos, R.; Delcher, A.; Dew, I.; Fasulo, D.; Flanigan, M.; Florea, L.; Halpern, A.; Hannenhalli, S.; Kravitz, S.; Levy, S.; Mobarry, C.; Reinert, K.; Remington, K.; Abu-Threideh, J.; Beasley, E.; Biddick, K.; Bonazzi, V.; Brandon, R.; Cargill, M.; Chandramouliswaran, I.; Charlab, R.; Chaturvedi, K.; Deng, Z. M.; Di Francesco, V.; Dunn, P.; Eilbeck, K.; Evangelista, C.; Gabrielian, A. E.; Gan, W.; Ge, W. M.; Gong, F. C.; Gu, Z. P.; Guan, P.; Heiman, T. J.; Higgins, M. E.; Ji, R. R.; Ke, Z. X.; Ketchum, K. A.; Lai, Z. W.; Lei, Y. D.; Li, Z. Y.; Li, J. Y.; Liang, Y.; Lin, X. Y.; Lu, F.; Merkulov, G. V.; Milshina, N.; Moore, H. M.; Naik, A. K.; Narayan, V. A.; Neelam, B.; Nusskern, D.; Rusch, D. B.; Salzberg, S.; Shao, W.; Shue, B. X.; Sun, J. T.; Wang, Z. Y.; Wang, A. H.; Wang, X.; Wang, J.; Wei, M. H.; Wides, R.; Xiao, C. L.; Yan, C. H. *Science* **2001**, *291*, 1304−1351.
(14) Carey, L.; Mitnik, L. *Electrophoresis* **2002**, *23*, 1386−1397.
(15) Peterson, N.; Alarie, J.; Ramsey, J. In *Micro Total Analysis Systems*; Northrup, A., Ed.; Kluwer Academic: Squaw Valley, CA, 2003; Vol. 1.
(16) Tegenfeldt, J. O.; Prinz, C.; Cao, H.; Huang, R. L.; Austin, R. H.; Chou, S. Y.; Cox, E. C.; Sturm, J. C. *Anal. Bioanal. Chem.* **2004**, *378*, 1678−1692.
(17) Han, J.; Turner, S. W.; Craighead, H. G. *Phys. Rev. Lett.* **1999**, *83*, 1688−1691.

10.1021/ac0710580 CCC: $37.00
Published on Web 09/21/2007

advances have been made in the area of separation materials for microcapillary electrophoresis and capillary injector designs and strategies. However, current miniaturized electrophoresis systems, in particular capillary electrophoresis (CE), rely upon the use of viscous polymer media as sieving matrices needed to separate DNA fragments of different lengths.[9] This is due to the typical, well-known insensitivity of DNA mobility to DNA molecule length in free solution.[26] Implementing automated chip-based gel electrophoresis systems for multiple, consecutive DNA separations remains limited by difficulties in loading and replacing viscous polymer gels in microchannels.[1] More recently, novel separation methods have been developed to analyze DNA without the use of sieving matrices. Craighead *et al.*[27] developed a nanochannel consisting of alternating thick and thin regions that differentially trap DNA based on length under an applied electric field. Also, there have been attempts to exploit the Brownian motion of DNA molecules to achieve size-dependent separation.[17−20] There has been significant interest in the transport of DNA molecules through nanopores as a possible fast sequencing technology, but in its current form the technology is not suitable for multiple oligonucleotide separations or sequencing.[22−24] Finally, end-labeled free-solution electrophoresis (ELFSE) of DNA has been performed in free solution by labeling the DNA with a large, uncharged molecule ("drag-tags") prior to electrophoresis.[28−30]

In this paper we demonstrate that gel-free electrokinetic separation of double-stranded deoxyribonucleic acid (dsDNA) can be effectively achieved in nanochannels. The advantages of this technique include small reagent volume, free-solution separation without DNA modification (other than labeling), and an order of 1 min analysis time. Nanoscale electrokinetic transport of liquid has been studied both theoretically and experimentally for the past several decades.[31−37] Our group recently showed that electrokinetic migration of charged species in nanochannels is strongly affected by valence-dependent segregation dynamics of the transverse electric fields associated with finite electrical double layers (EDLs).[34,35] We studied the electrokinetic transport both

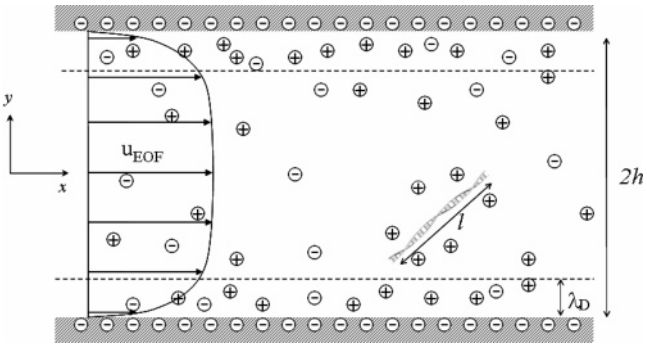

Figure 1. Schematic of nanochannel electrophoresis of rodlike oligonucleotides. Important length scales are the depth of the channel ($2h$), the length of the dsDNA (l), and the Debye length (λ_D).

of neutral and charged molecules in nanochannels. For ion transport in channels with finite EDL thickness, both streamwise and transverse electromigration fluxes contribute to the separation and dispersion dynamics of small analyte ions. Griffiths and Nilson presented theory for similar separation dynamics but with pressure-driven flow as a driving force.[38] Most relevant to the current work, Peterson *et al.* first showed that oligonucleotides can be separated via nanochannel electrophoresis[15] and postulated that steric effects alone would determine the residence time distribution for a mixture of 100−1000 base-pair (bp) oligonucleotides.

Although we are currently developing models for the dilute polyelectrolyte separation dynamics in nanochannels, we here report results from a parametric experimental study of transport and separation of dsDNA oligonucleotides in custom-fabricated fused-silica nanochannels using quantitative epifluorescence imaging techniques. We observe that the order of migration of dsDNA depends on the relative magnitude of the dsDNA molecular length and the EDL thickness, as well as the depth of the channel (see the schematic in Figure 1). As we shall discuss, these dependences suggest that steric effects alone cannot explain the differential migration rate of dsDNA in these channels. We present estimates of electrophoretic mobilities and separation selectivity based on measured, species-specific residence times.

EXPERIMENTAL METHODS AND MATERIALS

dsDNA Reagent Preparation. Oligonucleotides were synthesized using standard β-cyanoethyl phosphoramidite chemistry (Operon).[39] These molecules were then labeled incorporating a fluorescein moiety at the 5′ end of the sense strand during synthesis. Double-stranded species were generated by resuspending complementary oligonucleotides in 100 mM sodium borate buffer (Sigma, B-6768) titrated to pH 8.0 with NaOH (LabChem Inc., Pittsburgh, PA LC24500-2), then mixed in a ratio of 1:1 to obtain a final total concentration of 1 mM oligonucleotide. These strands were annealed in an iCycler PCR machine (BioRad) by boiling and subsequently cooling the samples from 95 down to 4 °C, decreasing 0.5 °C every 30 s. The 10, 25, 50, and 100 bp sequences were as follows:

10bp—CAGGAAACAG

(18) Han, J.; Craighead, H. G. *Science* **2000**, *288*, 1026−1029.
(19) Han, J.; Craighead, H. G. *J. Vac. Sci. Technol., A* **1999**, *17*, 2142−2147.
(20) Han, J. Y.; Craighead, H. G. *Anal. Chem.* **2002**, *74*, 394−401.
(21) Howorka, S.; Cheley, S.; Bayley, H. *Nat. Biotechnol.* **2001**, *19*, 636−639.
(22) Deamer, D. W.; Akeson, M. *Trends Biotechnol.* **2000**, *18*, 147−151.
(23) Meller, A.; Nivon, L.; Branton, D. *Phys. Rev. Lett.* **2001**, *86*, 3435−3438.
(24) Henrickson, S. E.; Misakian, M.; Robertson, B.; Kasianowicz, J. J. *Phys. Rev. Lett.* **2000**, *85*, 3057−3060.
(25) Lin, Y. W.; Huang, M. F.; Chang, H. T. *Electrophoresis* **2005**, *26*, 320−330.
(26) Viovy, J. L. *Rev. Mod. Phys.* **2000**, *72*, 813−872.
(27) Craighead, H. G.; Turner, S. W. P.; Han, J.; Cabodi, M. *Abstr. Pap.—Am. Chem. Soc.* **2001**, *222*, U191−U191.
(28) Vreeland, W. N.; Meagher, R. J.; Barron, A. E. *Anal. Chem.* **2002**, *74*, 4328−4333.
(29) Meagher, R. J.; Won, J. I.; McCormick, L. C.; Nedelcu, S.; Bertrand, M. M.; Bertram, J. L.; Drouin, G.; Barron, A. E.; Slater, G. W. *Electrophoresis* **2005**, *26*, 331−350.
(30) Won, J. I.; Meagher, R. J.; Barron, A. E. *Electrophoresis* **2005**, *26*, 2138−2148.
(31) Burgreen, D.; Nakache, F. R. *J. Phys. Chem.* **1964**, *68*, 1084−1091.
(32) Levine, S.; Marriott, J. R.; Neale, G.; Epstein, N. *J. Colloid Interface Sci.* **1975**, *52*, 136−149.
(33) Levine, S.; Marriott, J. R.; Robinson, K. *J. Chem. Soc., Faraday Trans. 2* **1975**, *71*, 1−11.
(34) Pennathur, S.; Santiago, J. G. *Anal. Chem.* **2005**, *77*, 6772−6781.
(35) Pennathur, S.; Santiago, J. G. *Anal. Chem.* **2005**, *77*, 6782−6789.
(36) Garcia, A. L.; Ista, L. K.; Petsev, D. N.; O'Brien, M. J.; Bisong, P.; Mammoli, A. A.; Brueck, S. R. J.; Lopez, G. P. *Lab Chip* **2005**, *5*, 1271−1276.
(37) Griffiths, S. K.; Nilson, R. H. *Anal. Chem.* **1999**, *71*, 5522−5529.
(38) Griffiths, S. K.; Nilson, R. H. *Anal. Chem.* **2006**, *78*, 8134−8141.
(39) Hagmar, P.; Bailey, M.; Tong, G.; Haralambidis, J.; Sawyer, W. H.; Davidson, B. E. *Biochim. Biophys. Acta* **1995**, *1244*, 259−268.

25bp—CAGGAAACAGCTATGACCATGATTA

50bp—CAGGAAACAGCTATGACCATGATTACGCCAAGCTATTTAGGTGACGCGTT

100bp—CAGGAAACAGCTATGACCATGATTACGCCAAGCTATTTAGGTGACGCGTTAGAATACTCAAGCTATGCATCAAGCTTGGTACCGAGCTCGGATCCACTAG.

Each double-stranded annealed species was mixed in an equal ratio, along with two additional identifiable species, sodium fluorescein (Sigma, F-6377) and fluorescein-12-UTP (UTP) (Enzo Life Sciences, 42834), which were also at a concentration of 1 mM in 100 mM sodium borate. The final ladder mixture contained species in equal concentration (167 μM) in 100 mM buffer.

To uniquely identify each detected species in the mixture after nanochannel separation, we compiled a calibration of the residence times for each component by performing experiments on mixtures where the initial concentration of one component was 5 times greater than that of all other components of the ladder (we refer to these as "spike" experiments). For these spike experiments we prepared solutions with 100 μM unspiked species, and 500 μM of the spiked species, each in 100 mM of buffer. (Table SI in the Supporting Information summarizes the initial and final concentrations of analyte and buffers.)

Nanochannel Fabrication. Experiments were carried out in simple-cross channels (shown in Figure 2a) and double-T (not shown) with a separation column length of 25 mm. We fabricated these channels within our group using conventional optical photolithography, dry chemical etching, and bonding techniques as previously reported.[35,40] Within the end-channel reservoir wells, we incorporated 1 μm diameter circular posts as filtering structures (these were confined to the wells alone and provided no separation). We also etched a separate channel system parallel to and within 100 μm of the separation channel to serve as reference marks.

We performed preliminary control experiments in a microchannel of 50 μm width and a centerline depth of 20 μm. For this, we used microchannels etched in low-fluorescence Borofloat glass microchips (Micralyne, Alberta, Canada) with a simple-cross channel. As described below, the control experiment showed no detectable separation over a 23 mm separation distance.

Instrumentation and Data Acquisition. A schematic of the experimental setup is shown in Figure 2b. We used a computer-controlled high-voltage (HV) power supply (Micralyne, Alberta, Canada) to apply chosen potentials to the four wells of each channel. The voltage scheme used for the dsDNA CE separation is shown in Figure 2a, where we indicate the voltage applied to each well during the two stages of the experiment: sample loading and injection/separation. The lengths of the north, south, west, and east (the separation) channels were, respectively, 3.5, 3.5, 11.4, and 24.6 mm. We used platinum wire as electrodes. We recorded fluorescence intensity using an inverted epifluorescent microscope (Olympus IX70) fitted with a water immersion objective lens with a magnification of 60× and a numerical aperture of 0.9 (Olympus, Inc.). We used an argon-ion 488 laser to illuminate the channel, and we filtered the peak absorption and emission wavelengths of 485 and 535 nm, respectively, with an XF100-3 filter cube (Omega optical, Brattleboro, VT). We recorded intensity images 20 mm downstream of the injection point using a cooled intensified charge-coupled device (ICCD) camera (I-PentaMAX, Gen III, Princeton Instruments) with a 512 × 512 CCD pixel array and 12-bit digitization. The exposure time was 10 ms at a frame rate of 16 Hz. We used on-chip binning of 10 × 10 pixels and regions of interest (ROIs) to create an 80 × 100 pixel detection "spot" for

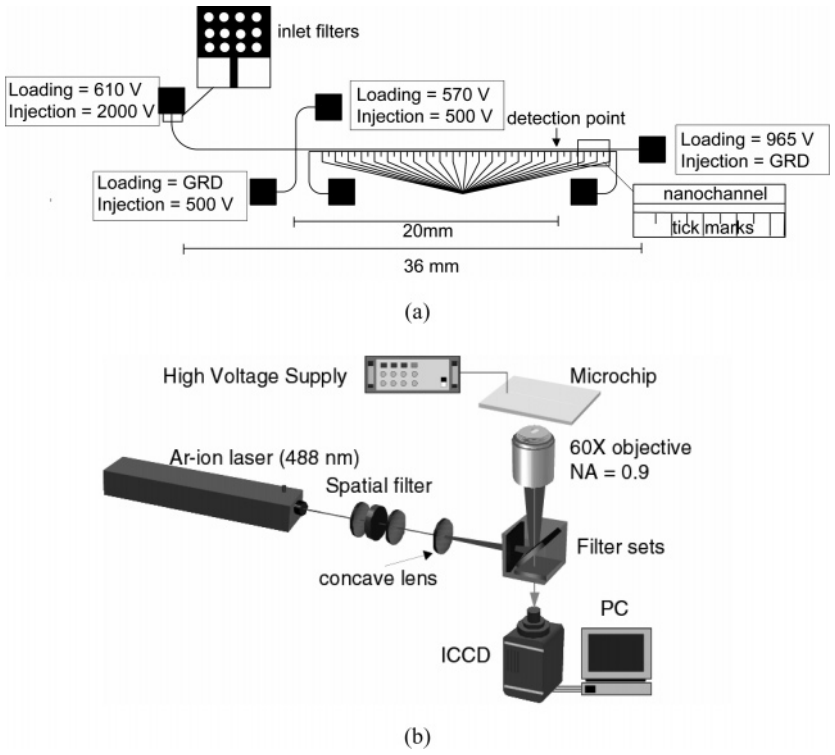

Figure 2. (a) Schematic of a typical nanochannel for the experiments reported in this paper. The detection area (30 μm × 30 μm) was centered at 20 mm to the right of the injection point. (b) Schematic showing the detection apparatus and setup used to collect image data for dsDNA separation experiments. The optical system includes an argon-ion 488 laser, an epifluorescent microscope, a water immersion objective lens with a magnification of 60× and a numerical aperture of 0.9, and a cooled intensified CCD camera.

high-sensitivity analysis. Win32 software (Roper Scientific, Trenton, NJ) was used to collect image data. We attempted using a photomultiplier tube (PMT) (Hamamatsu) in place of the CCD camera to gather image data. However, the signal-to-noise (S/N) ratio obtained using the PMT was consistently lower than that obtained using the CCD camera owing to the difficulty involved with aligning the PMT within the small depth of the nanochannel. We here used PMT data exclusively to compare to the ICCD data of the 1560 nm deep channels, for which alignment was easily achieved. We used in-house software written in LabVIEW 6i to control the HV power supply and the PMT.

Adsorption of dsDNA molecules onto the channel walls did not occur appreciably during the experiments. This was confirmed by direct observation of channel walls and by monitoring ionic current (Keithley 6314, Keithley, Inc.) during the experiments (note: ion current in a nanochannel is a strong function of wall charge density).

Experimental Conditions and Procedure. We performed a parametric study of gel-free electrophoresis in channels with three depths (40, 100, and 1560 nm), varying the background electrolyte (BGE) concentration from 1 to 100 mM (sodium borate). These conditions allowed us to achieve ratios of Debye length-to-channel depth ranging from 0.0006 to 0.2. Each sample mixture contained six species: fluorescein, UTP, and 10, 25, 50, and 100 bp dsDNA. Our use of the ICCD as a "point wise" detector yielded temporal electropherograms. Peaks in the electropherograms were identified using the spiked and unspiked comparisons. At a fixed BGE concentration, we performed six (spiked) experiments in which we increased each of the six species initial concentrations by 5-fold. For each BGE concentration, we also performed a seventh experiment in which all components were present in equal concentration (unspiked). The (applied) axial electric field in the separation section of the channel was kept constant at 200 V/cm, and the detection point was fixed 20 mm from the injection point. We observed no adsorption of fluorescent dsDNA molecules on the channel walls. Three realizations for each experiment were sufficient to reduce statistical uncertainty of measured (resolved) residence times to 7%. (A summary of the experiments performed is shown in Table SII of the Supporting Information).

Last, we describe our pre-experiment channel conditioning. We first filled the channels (via capillary action) with deionized (DI) water and stored them wet between experiments. We then effected electroosmotic flow (EOF) at an order of 200 V/cm for 150 s. Before each new BGE run, we flushed the channels with EOF of DI for 2 min. We then flushed with EOF of the new buffer for 2 min. We monitored ion current for each run. We note that we often observed slight upward drifts in measured current (order of 10% increases over 30 min runs) after introducing a new buffer. From current monitoring measurements, we estimate that electroosmotic mobilities remained constant to within approximately 5% over the experimental runs.

EXPERIMENTAL RESULTS AND DISCUSSION

We performed an initial validation of our dsDNA sample mixture using an acrylamide gel.[41] A brief discussion of these results is available in section A in the Supporting Information. Here we first show a comparison of gel-free electrophoresis in a microchannel versus a nanochannel at similar experimental conditions. Then, we present sample results of our study of oligonucleotide transport in nanochannels and show estimates of electrophoretic mobility that can be extracted from measured data. In the Supporting Information we also present results of selectivity, and we discuss error estimates.

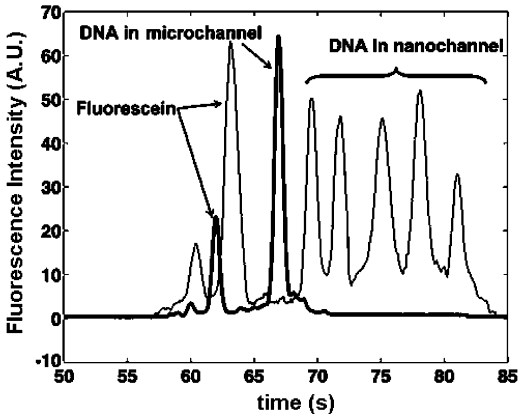

Figure 3. Electropherograms for free-solution DNA separation experiments in a 50 μm deep microchannel (thick line) and a 100 nm deep channel (thin line). The BGE concentration and applied field for both were 10 mM and 100 V/cm, respectively. Both experiments used the same sample solution (~167 μM dsDNA and fluorescein). The nanochannel clearly improves resolution.

Gel-Free Electrophoresis of dsDNA Oligonucleotides. Figure 3 shows two electropherograms (intensity measured at the detector as a function of time) of free-solution electrophoresis of the six species in 10 mM sodium borate buffer. The thick black line corresponds to the separation in the 50 μm $\times$ 20 μm microchannel and shows that no discernible separation of the dsDNA strands is achieved over a 23 mm separation. Fluorescein (peak at $\approx$62 s) is clearly separated from the unresolved DNA ladder peak at $\approx$67 s, as expected.

Also shown in this figure is the electropherogram (thin black line) that results from a separation experiment carried out in a 100 nm deep channel at the same BGE concentration and for a 20 mm separation distance. Again, the fluorescein peak appears first ($\approx$64 s). dsDNA peaks are clearly separated and resolved. The slight difference in the location of the fluorescein peak is expected due to the slightly different location of the detector and the difference in substrates (borosilicate for the microchannel and fused-silica for the nanochannel). Last in Figure 3, we note that there is a seventh peak that appears to the right of fluorescein. We attribute this to the behavior of fluorescin at pH $\sim$ 8.0, where fluorescein exists predominantly as a dianion in aqueous solution, yet in equilibrium with a small amount of its monoanion form. The fluorescein monoanion in solution has lower electrophoretic mobility; thus, it appears first at the detection point.

dsDNA Transport and Separation in Nanochannels. We here present quantitative measurements of dsDNA transport in channels of depth 40, 100, and 1560 nm. We begin by describing in detail one set of experiments in a 100 nm deep channel with constant BGE concentration at 10 mM. For all experiments (all concentrations and channel depths), EOF (toward the cathode) dominates over the anion analyte electrophoretic motion. The

(40) Pennathur, S. Doctorate of Philosophy, Stanford University, 2006.
(41) Brody, J. R.; Kern, S. E. *BioTechniques* **2004**, *36*, 214−216.

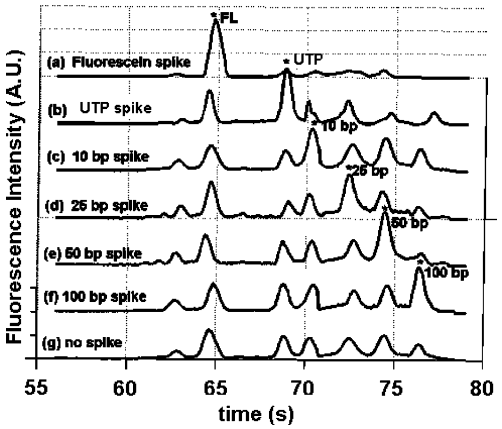

Figure 4. Measured electropherograms for electrokinetic separations of fluorescein, UTP, and a 10−100 bp oligonucleotide ladder in a 100 nm deep channel and a 10 mM sodium borate buffer. The various traces show results for a (a) fluorescein spike, (b) UTP spike, (c) 10 bp spike, (d) 25 bp spike, (e) 50 bp spike, (f) 100 bp spike, and (g) no spike.

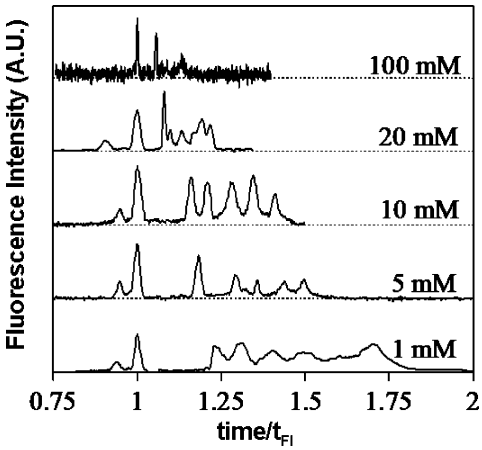

Figure 5. Measured electropherograms for electrokinetic separations of fluorescein, UTP, and a 10−100 bp oligonucleotide ladder in a 100 nm deep channel. Electropherograms are shown for separations in five different concentrations of sodium borate: 100 (top), 20, 10, 5, and 1 mM (bottom). t_{Fl} is the residence time of fluorescein in each experiment.

order of elution is affected by these two effects and may be a function of other effects (such as steric−wall interactions[42,43] and interactions with the finite velocity and electric field gradients in the finite EDL nanochannels).

We first show in Figure 4 seven electropherograms to illustrate the spiking technique. The top electropherogram shows a separation experiment where the initial fluorescein concentration is 5 times higher than the rest of the species. The subsequent five plots show electropherograms for spikes of UTP, and 10, 25, 50, and 100 bp oligonucleotides, respectively. The bottom electropherogram shows the case where all six species are initially present at approximately the same concentration. Figure 4 clearly demonstrates that the species separate under gel-free electrophoresis inside 100 nm deep channels. Separation time is less than 2 min.

Figure 5 shows the results of the normalized electropherograms from unspiked experiments for 100 nm deep channels and at each of the five buffer concentrations. Time is normalized by the residence time of fluorescein in each experiment from the 1 to 100 mM cases, these times are, respectively, 25.3, 35.8, 40.1, 75.4, and 118 s. Each peak was identified via six spiking experiments at each condition (not shown). (The low S/N ratio of the 100 mM case is most likely due to photobleaching of fluorescein that occurs because of longer residence time.) For all concentrations of sodium borate, both fluorescein and UTP peaks are well resolved. In 100 nm channels, the six components of the mixture were successfully separated for all buffer concentrations studied. Resolution between peaks is highest for 10 mM sodium borate. This suggests that there is an optimum condition, related to the EDL thickness, at which to carry out separations. For 10 mM sodium borate the order of elution is fluorescein (FL), UTP, and 10, 25, 50, and 100 bp oligonucleotides. This result is expected since the EDL is thin ($\lambda_D/h \approx 3\%$), and the electrophoretic mobilities are $\mu_{Fl} < \mu_{UTP} < \mu_{10bp} < \mu_{25bp} < \mu_{50bp} < \mu_{100bp}$. At higher concentrations of sodium borate (20 and 100 mM), we observe separation and the same order of elution as the 10 mM case (FL, UTP, 10, 25, 50, and 100 bp), yet the resolution was lower. This result is somewhat unexpected as increased sodium borate concentration reduces electroosmotic velocity, while residence time for all species increases. We would therefore expect an increased resolution between peaks, but we observed exactly the opposite behavior. One possible explanation is that resolution may be affected by changes in the bulk ion density. This effect plays a role since electrophoretic mobility decreases as the bulk ion concentration increases. For 5 mM sodium borate buffer concentration, where $\lambda_D/h \approx 4\%$, the separation resolution is good, and the order of elution is the same as for the 10 mM case. Last, for 1 mM sodium borate, the EDL is approximately 10% of the channel depth, and the order of elution is different than the higher BGE concentrations: FL, UTP, and 100, 50, 10, and 25 bp oligonucleotides, respectively. The 1 mM concentration results in the largest EDL thicknesses, where transverse electromigration may play a role in improving resolution. This is as expected from the work of Pennathur and Santiago[34] who analyzed the effect of EDLs on small ion transport in nanochannels. Apparently, for thick EDLs, the effects of ion density and coupling with EDL compete to determine the net axial migration rate. This suggests a significant coupling between bulk EOF, electromigration in the axial and transverse direction, and steric−wall interactions.

We performed experiments similar to that of Figure 5 for the 40 and 1560 nm deep channels. In Table 1 we summarize the observed order of elution of each species for all buffer concentrations and channel depths. Fluorescein is the smallest ion in the mixture, with the lowest reported electrophoretic mobility and valence. Its residence time is observed to be the shortest in all experiments. Similarly, UTP (also a relatively small molecule) is consistently the second molecule to reach the detector for all experiments where the separation is resolved. In contrast, the detection order of the 10, 25, 50, and 100 bp dsDNA oligonucleotides varies with experimental conditions. This fact alone suggests that the separation dynamics are a function of finite EDL physics. A list of the relevant physical process is likely to include electrophoretic mobility dependence on ionic strength, steric

(42) Blom, M. T.; Chmela, E.; Oosterbroek, R. E.; Tijssen, R.; van den Berg, A. *Anal. Chem.* **2003**, *75*, 6761−6768.
(43) Chmela, E.; Tijssen, R.; Blom, M.; Gardeniers, H.; van den Berg, A. *Anal. Chem.* **2002**, *74*, 3470−3475.

Table 1. Order of Migration of Oligonucleotide Strands in Various Channel Depth and Buffer Concentrations

channel depth	100 mM	20 mM	10 mM	5 mM	1 mM
1560 nm	FL, UTP, 100, 50, 25, 10	FL, UTP, others not resolved	FL, UTP, others not resolved	FL, UTP, 100, 50, 25, 10	FL, UTP, 100, 50, 25, 10
100 nm	FL, UTP, 10, 25, 50, 100	FL, UTP, 10, 25, 50, 100	FL, UTP, 10, 25, 50, 100	FL, UTP, 10, 25, 50, 100	FL, UTP, 100, 50, 10, 25
40 nm	FL, UTP, 10, 25, 50, 100	FL, UTP, 10, 25, 50, 100	FL, UTP, others not resolved	FL, UTP, others not resolved	FL, UTP, others not resolved

interactions between finite size dsDNA molecules and the channel walls, transverse electromigration and segregation of analytes, hydrodynamic interactions between molecules and walls, and interactions between molecules and the nonuniform electroosmotic velocities of finite EDLs.

In 1560 nm deep channels, for sodium borate concentrations of 1, 5, and 100 mM, where the EDL is very thin ($0.0006 < \lambda_D/h < 0.006$), the order of elution of the dsDNA strands is consistently 100, 50, 25, and 10 bp oligonucleotides. These results are in apparent contradiction with the accepted view that the electrophoretic mobility of oligonucleotides of 10−400 bp increases with increasing number of base pairs.[44] Reported values of oligonucleotide electrophoretic mobility (in gel-free solutions) show a 9% increase between 10 and 100 bp (Figure 4 in ref 44). For thin EDLs, electrostatic repulsion forces (from the negatively charged walls) are negligible across the vast majority of the channel depth, and EOF velocities are approximately uniform (except for the thin EDL itself). Therefore, dsDNA molecules are expected to be approximately uniformly distributed throughout the channel depth. Furthermore, steric interactions with the walls are minimal since $l/h < 0.044$; thus, shear-induced migration toward the channel center and flow-field fractionation effects are negligible. One possible explanation for this is that the mobility is strongly affected by the fluorescein-5-isothiocyanate (FITC) (isomer I) label. In free solution, inclusion of FITC apparently increases the electrophoretic mobility of dsDNA as it increases the net ratio of charge to molecular weight. Since only a single FITC is incorporated per dsDNA strand, the net charge increase presumably affects the mobility of short dsDNA more strongly than that of longer dsDNA. Last, we note that the resolution was not sufficient to yield separation at the point of detection for BGE concentrations of 10 and 20 mM.

Results from experiments in 40 nm deep channels show that separation of a dsDNA ladder was achieved within our setup at the two higher BGE concentrations ($0.05 \leq \lambda_D/h$) and that the order of elution was consistently 10, 25, 50, and 100 bp oligonucleotides, respectively. These results are consistent with elution in thin-EDL conditions. For sodium borate concentrations ≤10 mM, fluorescein and UTP separated, but the separation resolution for dsDNA ladder was not sufficient.

Electrophoretic Mobility Estimates Based on Nanochannel Separation Data. Here we present estimates of the electrophoretic mobilities of the various components of the mixture (obtained from experimental separation data), and we compare these to literature values. Righetti et al.[44] review recent UV absorbance dsDNA mobility measurements obtained using gel-free, capillary zone electrophoresis. They show that dsDNA mobility is independent of molecular weight (number of base pairs) for molecules longer than ≈400 bp. dsDNA mobility decreases (continuously) for shorter molecules: for 100 bp molecules $\mu_{100bp} \approx 3.67 \times 10^{-8}$ m^2/(V s), and for 10 bp molecules, $\mu_{10bp} \approx 3.31 \times 10^{-8}$ m^2/(V s). We use a value of fluorescein mobility of 3.4×10^{-8} V/m/s (at a BGE concentration of 10 mM[45−47]), but we could not find published values for the mobility of UTP conjugated with fluorescein.

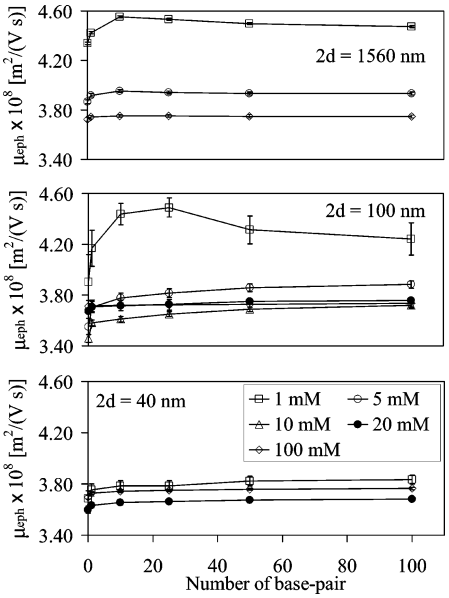

Figure 6. Plots of effective mobility as a function of dsDNA base pair length for different BGE concentrations (and λ_D/h): (top) h = 1560 nm, (middle) h = 100 nm, (bottom) h = 40 nm. Error bars are standard error. All experiments were performed with an applied axial electric field of E = 200 V/cm in the separation column with a detection point 20 mm downstream from the injection point.

In Figure 6 we show estimates of the electrophoretic mobility as a function of analyte molecular weight (number of base pairs). As a comparison, for the fluorescein and UTP data we used values for effective "base pairs" of zero and one, which are approximate extrapolations from the molecular weight of these molecules. Details of the calculation of mobility are given in section B in the Supporting Information. The error bars indicate standard error

(44) Righetti, P. G.; Gelfi, C.; D'Acunto, M. R. *Electrophoresis* **2002**, *23*, 1361−1374.

(45) Jacobson, S.; Hergenroder, R.; Koutny, L.; Ramsey, J. *Anal. Chem.* **1994**, *66*, 1114−1118.

(46) Whang, C. W.; Yeung, E. S. *Anal. Chem.* **1992**, *64*, 502−506.

(47) Bharadwaj, R.; Santiago, J. G.; Mohammadi, B. *Electrophoresis* **2002**, *23*, 2729−2744.

obtained by propagating the measured variance in residence times, as detailed in section C in the Supporting Information. In Figure 6 (top) we present data for the 1560 nm channel depth and for BGE concentrations of 1, 5, and 100 mM. At a BGE concentration of 100 mM, mobility is largest for 100 bp and smallest for 10 bp, but approximately constant at a value of 3.75×10^{-8} m^2/(V s). These mobility values and trends are in good agreement with published data for a dsDNA.[44] At BGE concentrations of 1 and 5 mM, we observed slight increase in mobility of the 10 and 25 bp molecules with respect to larger molecules. We again attribute this to the inclusion of (negatively charged) FITC fluorophore at the 5′ end which may substantially increase the electrophoretic mobility magnitude of short dsDNA strands. At BGE concentrations of 1 and 5 mM we observed that the mobility estimates are higher than expected. We do not have a physical explanation for these observations, except to note that these results are perhaps an artifact of the value of ζ-potential chosen to estimate $\langle u_{EOF} \rangle$. From Figure 2 of ref 35 we see that eq B1 overestimates the measured value of ζ-potential at low concentrations. Overestimating ζ results in a larger calculated electroosmotic velocity and a larger estimate of the electrophoretic mobility. In 100 nm deep channels (Figure 6 (middle)), at BGE concentrations equal to 20 and 100 mM, the estimated mobilities are approximately constant within the range of $3.71-3.75 \times 10^{-8}$ m^2/(V s). At BGE concentrations of 5 and 10 mM we observed a decrease in mobility with decreasing number of base pairs (a difference of approximately 4% between 100 and 10 bp, in line with the published values). More important for applications (separations) is the observation that mobilities of 10 and 25 bp molecules are ~5% larger than those of 50 and 100 bp. In 40 nm deep channels (Figure 6 (bottom)), calculated mobilities fall in a narrow range: from 3.65×10^{-8} to 3.83×10^{-8} m^2/(V s). For all BGE concentrations studied, mobility decreases with decreasing number of base pairs. In section D of the Supporting Information we also show the separation selectivity data for these experiments.

CONCLUSIONS

The primary result of this work is the experimental demonstration that small molecules and short dsDNA molecules can be separated by gel-free electrophoresis in nanochannels. Fluorescently labeled dsDNA molecules ranging from 10 to 100 base pairs were separated in less than 120 s in channels of depth ranging from 40 to 1560 nm. Further, we found that the observed migration times for different size oligonucleotide molecules depend on both l/h and λ_D/h. The dependence of effective mobility on λ_D/h suggests that interaction between dsDNA and the EDL is an important mechanism for determining effective mobility. These observations suggest that DNA separation is a result of the coupling of physics due to the polyelectrolyte nature of DNA molecules with EDL physics, as well as steric and hydrodynamic effects due to confinement. Effective electrophoretic mobility estimates obtained from residence time data agree well with literature values at sodium borate concentrations equal to or greater than 10 mM. At BGE concentration of 1 and 5 mM the mobility estimates are higher than previously reported values. Also, the presence of FITC at the 5′ end sense strand may significantly increase the magnitude of the electrophoretic mobility of short (10 and 25 bp) dsDNA strands. Separation selectivity is highest in 100 nm deep channels, for BGE concentrations (sodium borate) of 1−10 mM. In this channel and BGE, selectivity is smallest for 10 and 25 bp dsDNA oligonucleotides and higher for shorter and longer molecules.

ACKNOWLEDGMENT

This work is sponsored by the National Institutes of Health (Grant N01-HV-28183) and by a National Science Foundation PECASE Award (J.G.S., CTS-0239080-001). P.J.U. and J.G.S. were supported by NHLBI Proteomics contract N01-HV-28183. P.J.V. was also supported by a gift from the Floren Family Foundation. M.G.K. is funded by the Stanford Medical Scientist Training Program (MSTP) and the FFF. J.B.S. was supported by the Center for Clinical Immunology as Stanford (CCIS) Research Program.

SUPPORTING INFORMATION AVAILABLE

Separation and identification of species in our dsDNA sample mixture by gel-electrophoresis (section A), electrophoretic mobility estimates (section B), separation selectivity (section C), error estimates (section D), summary of stock and final concentrations of analyte and buffers (Table SI), and list of experimental parameters that were varied (Table SII). This material is available free of charge via the Internet at http://pubs.acs.org.

Received for review May 22, 2007. Accepted July 17, 2007.

AC0710580